# Electron Localization Function in Full-Potential Representation for Crystalline Materials

**A. Ormeci,* H. Rosner, F. R. Wagner, M. Kohout, and Yu Grin**

*Max-Planck-Institut für Chemische Physik fester Stoffe, Nöthnitzer Strasse 40, 01187 Dresden, Germany*

*Received: August 22, 2005; In Final Form: November 10, 2005*

The electron localization function (ELF) is implemented in the first-principles, all-electron, full-potential local orbital method. This full-potential implementation increases the accuracy with which the ELF can be computed for crystalline materials. Some representative results obtained are presented and compared with the results of other methods. Although for crystal structures with directed bonding only minor differences are found, in simple elemental metals, there are differences in the valence region, which give rise to different ELF topologies.

## 1. Introduction

The electron localization function (ELF) was introduced by Becke and Edgecombe[1] as a tool to identify regions where electrons are localized in atomic and molecular systems. Savin et al.[2] suggested an alternative interpretation of the original ELF expression, which justified the calculation of ELF by density functional theory-based methods. Since then, ELF has been widely used to study chemical bonds in both molecules and solids.[3−5] Most recently, a pair density functional called the electron localizability indicator (ELI) was proposed.[6] Within the framework of this approach, we interpret ELF as an approximation to ELI for the single-determinantal ansatz.

The ELF distribution, $\eta(\vec{r})$, is given by $\eta(\vec{r}) = 1/[1 + \chi^2(\vec{r})]$, where

$$\chi(\vec{r}) = \frac{\frac{1}{2}\sum_i^{\text{occ}} |\vec{\nabla}\psi_i|^2 - \frac{1}{8}\frac{(\vec{\nabla}\rho)^2}{\rho}}{\frac{3}{10}(3\pi^2)^{2/3}\rho^{5/3}} \qquad (1)$$

The numerator in eq 1 involves the gradients of (i) the crystal wave functions, $\psi_i(\vec{r}) \equiv \psi_{\nu\vec{k}}(\vec{r})$, with band index $\nu$ and wavevector $\vec{k}$ and (ii) the total charge density, $\rho(\vec{r})$. Furthermore, the features of chemical bonding are investigated by a topological analysis of the ELF distribution, which requires the gradient and higher derivatives of the ELF to be computed.[7] Therefore, the ELF must be accurately calculated in order to avoid two possible pitfalls: (i) occurrence of spurious maxima and (ii) missing a genuine maximum due to interpolation. The former case may occur in regions where the crystal wave functions and hence the charge density are poorly represented, e.g., in the interatomic regions in methods based on the atomic sphere approximation (ASA). The latter case may show up in methods that treat the charge density differently inside (in terms of spherical harmonics) and outside (in terms of plane waves) the muffin tin spheres, since in these methods there is always a certain mismatch of the charge density at sphere boundaries.

Most of the ELF analyses reported on crystalline materials have been performed by using the LMTO ASA. It is well-known that electronic structure calculation methods that make no shape approximations to the charge density (or to the potential), full-potential methods as commonly called, have been more accurate than the ASA versions regarding the total energy and other physical quantities. Thus, it is conceivable that a full-potential calculation of the ELF should yield more accurate ELF values resulting in a more reliable chemical-bonding analysis via ELF in crystalline materials within the density functional theory.[8] However, there is an important difference between ELF and total energy: ELF is a local quantity whose computation does not involve integrations over the position space. Although more accurate charge density and crystal wave functions, $\psi_{\nu\vec{k}}(\vec{r})$, are implied according to variational principle, when the accuracy in total energy is increased, the extent of improvement in the calculation of a local quantity such as ELF cannot be estimated in advance. With this in mind, it is still important to be able to calculate the ELF with a computational scheme containing fewer approximations. In addition, it is preferable that in the chosen method the whole space is treated in a uniform manner (no division of space into spheres and interstitial).

In light of these considerations, we have implemented ELF in the first-principles, all-electron, full-potential local orbital minimal basis method (FPLO).[9] Here, we report some representative results of the ELF calculations obtained by our FPLO implementation and compare them with their counterparts obtained by using the tight-binding, linear muffin tin orbital method within atomic sphere approximation (TB-LMTO-ASA).[10,11] These comparisons show that the results can be divided into three groups: (i) materials for which there is basically no difference between the TB-LMTO ASA and the FPLO calculations, (ii) materials for which there are minor differences, and (iii) materials for which FPLO gives different valence attractors in regions of flat ELF distributions whereas in the TB-LMTO-ASA calculations one finds well-defined ELF maxima instead (see below, the discussion on fcc-Al metal).

## 2. ELF Implementation into the FPLO Method

The FPLO method[9] is based on a minimal basis approach where each atomic orbital *nl* with principal quantum number *n* and angular momentum *l* is represented by one basis function only. Basis functions in the FPLO method are atomic orbital-

* To whom correspondence should be addressed. E-mail: ormeci@cpfs.mpg.de.

10.1021/jp054727r CCC: $33.50 
Published on Web 12/31/2005

like having the form:

$$\phi_{\vec{R}\vec{s}nL}(\vec{r}) = \phi_{\vec{R}\vec{s}nL}(|\vec{r} - \vec{s}|)Y_l^m(\vec{r} - \vec{s})$$

where, $\vec{R}$ is a lattice translation vector, $\vec{s}$ denotes atomic sites in the unit cell, and $L$ stands for the $lm$ pair, $m$ being the magnetic quantum number. The basis functions for each crystallographically different atom are obtained by solving an effective Schroedinger equation, which contains the spherically averaged crystal potential and an artificial confining potential of the form $(r/r_0)^N$.[12] This confining potential forces the basis functions to be more strongly localized than the atomic orbitals. In this expression, $N$ is set to 4 by default, but it can be treated as a variational parameter with respect to the total energy, as well. The value of $N$ is the same for all basis functions. The quantity $r_0$ is proportional to the nearest-neighbor distance, and the proportionality constant $x_0$ is specified separately for each basis function. For genuine valence basis functions, the values of $x_0$'s are optimized during the self-consistency cycle. Regarding the orbitals used for semicore and polarization states, the $x_0$'s have fixed values chosen by the user. The extent of valence basis functions in a typical FPLO calculation is three times the average Wigner−Seitz radius. The crystal wave function labeled by band index $\nu$ and wavevector $\vec{k}$ is given as a linear combination of Bloch functions:

$$\psi_{\nu\vec{k}}(\vec{r}) = \sum_{R\vec{s}nL} c_{\vec{s}nL}^{\nu\vec{k}}\, e^{i\vec{k}\cdot(\vec{R}+\vec{s})}\, \phi_{\vec{R}\vec{s}nL}(\vec{r})$$

The Hamiltonian whose matrix elements enter into the eigenvalue equation contains all of the symmetry-allowed spherical harmonics of the potential, $V_{lm}$, up to some maximum orbital angular momentum value, $l_{\max}$ (currently, $l_{\max}$ is set to 12 by default). The charge density, $\rho(\vec{r}) = \sum_{\nu\vec{k}}^{\text{occ}}|\psi_{\nu\vec{k}}(\vec{r})|^2$, is also expressed in terms of site-centered spherical harmonics:

$$\rho(\vec{r}) = \sum_{\vec{s},L} \rho_{\vec{s},L}(|\vec{r} - \vec{s}|)\, Y_l^m(\vec{r} - \vec{s}) \qquad (2)$$

In our ELF implementation, the charge density $\rho(\vec{r})$ and its gradient $\vec{\nabla}\rho(\vec{r})$ are calculated directly from the basis functions. The charge density expression in eq 2 is not used. This is done to ensure the consistency between the two terms forming the numerator in eq 1.

A fundamental characteristic of the FPLO method is the absence of atomic (or muffin tin) spheres. In the FPLO formulation, the whole space is treated in a uniform manner, which makes charge density continuous at all points. In the context of ELF calculations, this is a clear advantage when compared with the muffin tin sphere-based methods. In the TB-LMTO-ASA method, overlapping atomic spheres are used, since the total volume of the atomic spheres should be equal to the unit cell volume. This constraint necessitates the occurrence of interstitial regions between atomic spheres, where the basis functions and hence the charge density are less accurate. In cases where these interstitial voids become too large, the so-called empty (or interstitial) spheres can be introduced. Because chemical bonding may take place in these parts of the crystal structure, the ELF calculated by the TB-LMTO-ASA method may be less accurate especially in open crystal structures.

On the other hand, in the full-potential implementations, full-potential linear muffin tin orbital (FP-LMTO) or full-potential linear augmented plane-wave (FP-LAPW) methods, charge density and potential are represented differently in the interstitial region and inside the nonoverlapping atom-centered spheres. The resulting mismatch of the charge density at sphere boundaries implies a discontinuity in the radial derivative of the charge density, and this may cause problems depending on how this discontinuity is handled when the gradient of the density is being evaluated.

The level of accuracy with respect to total energies in the FPLO method is comparable to that of the other all-electron, full-potential methods. Comparisons of the FPLO results regarding total energy, equilibrium lattice constants, bulk moduli, and magnetic moments with the corresponding quantities computed by the WIEN code[13] were reported in the original FPLO publication.[9] Similar comparisons between the FPLO and the WIEN codes concerning band structures, densities of states, and Fermi surfaces were also reported.[14,15] Total energies are typically found to be in agreement within a few milliHartrees per atom, and there are no significant differences in other physical quantities reported. In general, the FPLO program has been used successfully in various electronic structure studies.[16] Hence, the FPLO method offers a suitable computational platform for accurate calculations of ELF for crystalline materials.

## 3. Results and Discussion

For a selected set of crystalline compounds, we calculated the ELF by using the FPLO and TB-LMTO-ASA methods within the local density approximation (LDA).[17] Regarding the LDA exchange-correlation functionals, Perdew−Wang[18] and von Barth−Hedin[19] parametrizations were used in the FPLO and TB-LMTO-ASA calculations, respectively. For a few crystal structures, we calculated the ELF by using three different parametrizations of the exchange-correlation functional, Perdew−Wang, von Barth−Hedin, and Perdew−Zunger,[20] with the FPLO method. The ELF topologies were found to be unchanged in these cases. In the TB-LMTO-ASA calculations, the positions and radii of the empty spheres, whenever necessary, were determined using the procedure proposed by ref 21. Likewise, for the radii of the atomic spheres, the automatically determined values were used. In the FPLO calculations, the number of points on the radial grid was set to 400, twice the default value. Test calculations up to 1200 radial grid points were carried out on various crystal structures, and no changes in ELF topology were found. Convergence criteria used for self-consistency were $10^{-6}$ for density and $10^{-8}$ for total energy. The FPLO basis functions employed in the calculations are discussed below separately for each case.

The materials that we have chosen can be grouped as (i) materials containing covalent bonds (C in diamond form, C in graphite form, and $MgB_2$) and (ii) elemental metals (bcc-Li, fcc-Cu, and fcc-Al). The latter can be expected to be favorite cases for the LMTO-ASA application as they have closed-packed structures. The topological analysis of the ELF was done by the Basin package.[22] We will be interested mainly in comparing the ELF bonding attractors, because both computational schemes give the same results for the values of the core attractors and the properties (volume and integrated charge) of the corresponding core basins.

**3.1. Covalently Bonded Materials.** Carbon in diamond structure and $MgB_2$ are chosen as being good examples for covalently bonded materials. Regarding the LMTO-ASA application, the former is an open structure (packing fraction 34%) requiring empty spheres whereas the latter does not need any empty spheres. Graphite also has a quite simple picture of chemical bonding, but the severe openness of its crystal structure (packing fraction 17%) may pose difficulties in ELF calculations.

**TABLE 1: Values of the ELF Bonding Attractors and the Electron Count in Each Bond Basin**

| crystal | FPLO | LMTO-ASA | electron count |
|---|---|---|---|
| C (diamond) | 0.940 | 0.954 | 1.9 |
| C (graphite) | 0.945 | 0.954 | 2.6 |
| $MgB_2$ | 0.913 | 0.927 | 2.6 |

The values of the ELF bonding attractors as calculated by both methods at the experimental volumes are listed in Table 1, and ELF isosurfaces are shown in Figure 1. The lattice parameters used in the calculations are as follows: for diamond, $a = 3.567$ Å;[23] for graphite, $a = 2.461$ Å and $c = 6.709$ Å;[24] and for $MgB_2$, $a = 3.0851$ Å and $c = 3.5216$ Å.[25] In all cases, the ELF bonding attractors are found to be located at the midpoints of the closest C−C or B−B contacts. The amount of charge contained in each of the corresponding basins is the same in both calculations within the errors of integration.

The FPLO basis set used in the $MgB_2$ calculation consisted of the following: (i) Mg: 2*s*, 2*p* as semicore, 3*s*, 3*p*, 3*d*; (ii) B: 1*s* as semicore, 2*s*, 2*p*, 3*d*. The basis set for C in diamond structure used 1*s* as semicore and 2*s*, 2*p*, 3*d* as valence. Regarding the C in graphite structure, however, this basis set proved to be inadequate. Because of the highly anisotropic nature of graphite (layered structure), one should use 3*p* basis functions instead of the 3*d* to be able to account for the interlayer interaction correctly. Normally, for a given *nl* atomic orbital, there is only one radial basis function. Therefore, the extent of the $p_z$ orbital is essentially given by the extent of the radial 2*p* function, which is mainly determined by the intralayer interactions. This implies that the $2p_z$ function is relatively short-ranged and cannot provide an accurate description of the interlayer interaction. The 3*p* functions are needed to cure this inadequacy. The total energies and the results of the ELF calculations are in perfect agreement with these considerations. The total energy is lower by 0.93 eV per C atom when 3*p* is used instead of 3*d*. The basis set identical to that of the diamond structure gave two ELF bonding attractors split along the *c*-axis around the midpoint of each C−C nearest-neighbor pair. The expected ELF pattern was obtained when the 3*d* was replaced by 3*p*. The final result presented here was obtained by using both 3*p* and 3*d* basis functions.

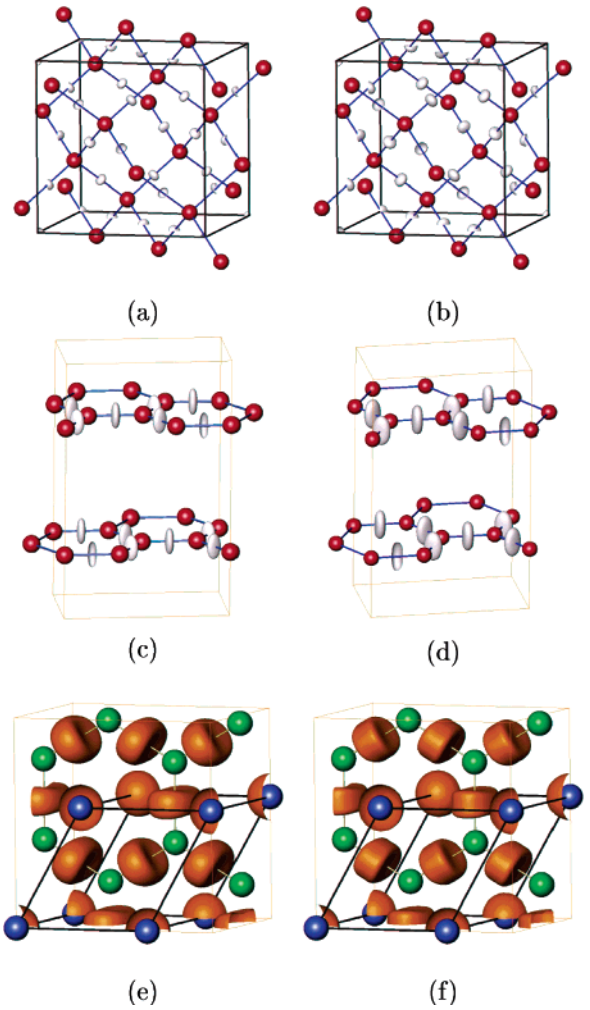


**Figure 1.** ELF isosurfaces in diamond (C, red) as computed by (a) FPLO ($\eta = 0.93$) and (b) TB-LMTO-ASA ($\eta = 0.94$); in graphite (C, red) as computed by (c) FPLO ($\eta = 0.92$) and (d) TB-LMTO-ASA ($\eta = 0.91$); and in $MgB_2$ (Mg, blue; B, green) as computed by (e) FPLO ($\eta = 0.75$) and (f) TB-LMTO-ASA ($\eta = 0.75$). Core regions are omitted for clarity of presentation.

**3.2. Elemental Metals.** Among the different types of chemical bonds, the metallic bond has been the most elusive one. In metals, the atoms have high coordination numbers but relatively few valence electrons. Therefore, one would expect to find multicenter bonds. Li and Cu are chosen as the bcc and fcc representatives, respectively, for this view. There is also an alternative view dating back to Pauling,[26] which regards the metallic bond as a partial (or unsaturated) bond between the nearest neighbors. According to our TB-LMTO-ASA calculations and the previously reported results,[27] Al has ELF bonding attractors at the midpoints of the closest Al−Al contacts with the electron count of 0.5 each. This makes the Al metal a representative case for the "partial covalent bond" view. On the other hand, because Al is usually regarded as the best material for the nearly free-electron model (see, for example, ref 23), it is very difficult to accept the bonding in Al in terms of directed or two-center bonds. Consequently, we have included Al in our study in order to find out whether full-potential treatment will give a picture of multicenter bonding.[28]

In this section, we will concentrate first on Li and Cu, and the case of Al will be discussed separately in the following section. Table 2 lists the results that we obtained by using FPLO and TB-LMTO-ASA together with the CRYSTAL[29] [Hartree−Fock (HF) level] results published earlier by Silvi and Gatti.[27] The FPLO and TB-LMTO-ASA calculations were carried out at the experimental volumes with $a_{Li} = 3.491$ Å, $a_{Cu} = 3.61$ Å, and $a_{Al} = 4.05$ Å.[23] The lattice parameters used in the CRYSTAL calculations are 3.5093, 3.61496, and 4.0862 Å, respectively.[27]

For the bcc-Li, the HF CRYSTAL and TB-LMTO-ASA methods find bonding attractors at the same positions, (6*b*) 0, 1/2, 1/2 (Figure 2b). Because these positions are at the centers of octahedral holes, the HF CRYSTAL and TB-LMTO-ASA methods predict six-center bonds in Li. In the FPLO calculation, attractors occur at positions (12*d*) 1/4, 0, 1/2 (Figure 2a), which can be interpreted as a 4-fold splitting and shifting of the attractor from the former location at the center of an octahedral hole toward the tetrahedral voids. The basins of these (12*d*) attractors contain about one-sixth of an electron each, and they imply four-center bonds. Although the ELF topology predicted by FPLO is different, the description of bonding that can be inferred from all of these three calculations has the common aspect that bonding is multicentered (four-center vs six-center).

ELF isosurfaces for fcc-Cu are shown in Figure 2c,d, respectively, as computed by the FPLO and TB-LMTO-ASA methods. The FPLO basis set consisted of 3*s*, 3*p* functions as semicore and 4*s*, 4*p*, 3*d*, 4*d* functions as valence. Because in

**TABLE 2: Values and Positions of the ELF Bonding Attractors**

| | FPLO | | LMTO-ASA | | HF-CRYSTAL | |
|---|---|---|---|---|---|---|
| crystal | position | ELF | position | ELF | position | ELF |
| Li-bcc | (12*d*) 1/4, 0, 1/2 | 0.6393 | (6*b*) 0, 1/2, 1/2 | 0.6284 | (6*b*) 0, 1/2, 1/2 | 0.637 |
| Cu-fcc | (8*c*) 1/4, 1/4, 1/4 | 0.3032 | (8*c*) 1/4, 1/4, 1/4 | 0.2631 | (4*b*) 1/2, 1/2, 1/2 | 0.38 |
| | | | | | (8*c*) 1/4, 1/4, 1/4 | 0.20 |
| Al-fcc | (32*f*) *x*, *x*, *x* $x = 0.19$ | 0.5992 | (24*d*) 0, 1/4, 1/4 | 0.6108 | (24*d*) 0, 1/4, 1/4 | 0.617 |

Cu the 3*d* states are almost fully occupied (more than nine electrons according to the *nl*-decomposition of the charge), 4*d* basis functions are necessary to provide the *d* character for the crystal wave functions. It should be noted that omission of the 4*d* basis functions results in a higher total energy and gives a different ELF topology. For Cu FPLO and TB-LMTO-ASA, methods agree with each other quite well by yielding a single set of identical attractor positions, (8*c*), while the HF CRYSTAL finds two sets of ELF bonding attractors. The set associated with the higher ELF value occurs at (4*b*), and the lower ELF value positions are reported to be (8*c*). In both the FPLO and the TB-LMTO-ASA calculations, each bonding basin holds about 1.05 electrons and represents a four-center bond. This implies that each Cu atom contributes 2.1 electrons to its chemical bonds in total.

**3.3. Case of Al.** As stated above, the HF CRYSTAL and TB-LMTO-ASA methods both predict ELF bonding attractors at the midpoints of the nearest neighbors (Table 2 and Figure 2f). The FPLO result listed in Table 2 for Al is obtained by using the default value, $N = 4$, for the exponent of the confining potential and the standard basis set: 2*s*, 2*p* as semicore, 3*s*, 3*p*, 3*d* as valence. The ELF attractors at the (32*f*) positions (Figure 2e) have monosynaptic basins. Because monosynaptic basins are traditionally associated with lone pairs,[30] this finding is very surprising. To gain some insight into this result, those aspects of the FPLO method that directly affect the quality of the crystal wave functions should be analyzed. First of all, it is of interest to observe how the ELF topology in Al evolves as the value of $l_{max}$ is varied. Second, the effects of (i) the orbitals included in the basis set and (ii) the exponent $N$ of the confining potential (since the confining potential influences the shape and the effective range of the basis functions) should be explored to see if the obtained ELF topology is stable.

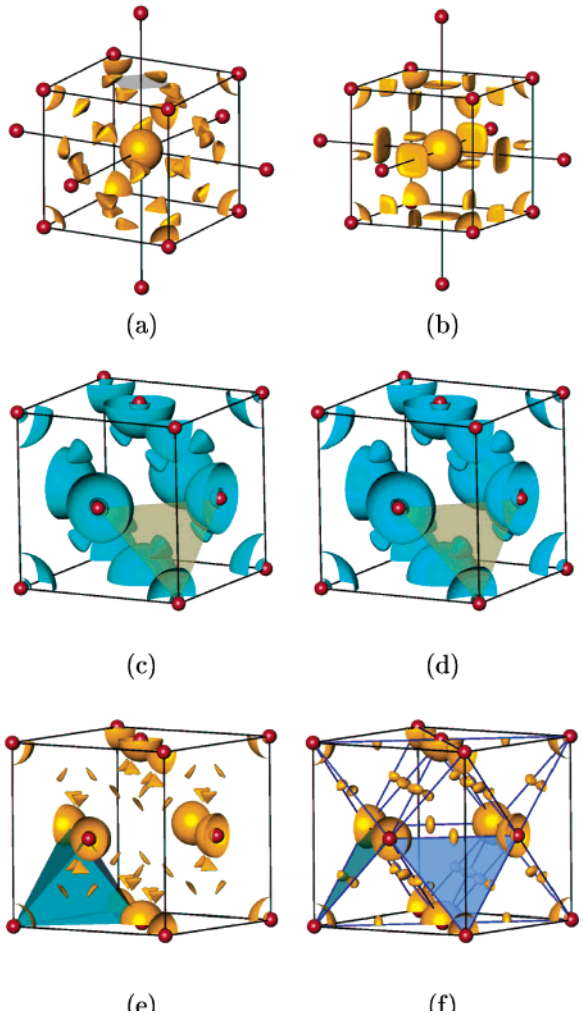


**Figure 2.** ELF isosurfaces in Li as computed by (a) FPLO ($\eta = 0.635$) and (b) TB-LMTO-ASA ($\eta = 0.622$); in Cu as computed by (c) FPLO ($\eta = 0.285$) and (d) TB-LMTO-ASA ($\eta = 0.255$); and in Al as computed by (e) FPLO ($\eta = 0.598$) and (f) TB-LMTO-ASA ($\eta = 0.603$). Red spheres denote atomic positions.

**TABLE 3: Values and Positions of the ELF Valence Attractors and Saddle Points Together with the Total Energy (in Units of Hartree per Atom) as a Function of $l_{max}$ for Al at Experimental Volume Calculated by Using the FPLO Standard Basis Set and $N = 4$**

| | | attractor | attractor | saddle point | |
|---|---|---|---|---|---|
| $l_{max}$ | energy | value | positon | value | position |
| 0 | −241.917668 | 0.6170 | (48*g*) *x*, 1/4, 1/4 | 0.6156 | (24*d*) 0, 1/4, 1/4 |
| | | 0.6144 | (32*f*) *x*, *x*, *x* | 0.6129 | (96*k*) *x*, *x*, *z* |
| 4 | −241.916693 | 0.5946 | (48*g*) *x*, 1/4, 1/4 | 0.5944 | (24*d*) 0, 1/4, 1/4 |
| | | 0.5827 | (32*f*) *x*, *x*, *x* | 0.5826 | (96*k*) *x*, *x*, *z* |
| 6 | −241.918251 | 0.5983 | (48*g*) *x*, 1/4, 1/4 | 0.5973 | (96*k*) *x*, *x*, *z* |
| | | 0.5982 | (32*f*) *x*, *x*, *x* | 0.5915 | (24*d*) 0, 1/4, 1/4 |
| 8 | −241.918299 | 0.5990 | (32*f*) *x*, *x*, *x* | 0.5969 | (48*g*) *x*, 1/4, 1/4 |
| | | | | 0.5887 | (24*d*) 0, 1/4, 1/4 |
| 10 | −241.918299 | 0.5993 | (32*f*) *x*, *x*, *x* | 0.5971 | (48*g*) *x*, 1/4, 1/4 |
| | | | | 0.5889 | (24*d*) 0, 1/4, 1/4 |
| 12 | −241.918298 | 0.5992 | (32*f*) *x*, *x*, *x* | 0.5971 | (48*g*) *x*, 1/4, 1/4 |
| | | | | 0.5885 | (24*d*) 0, 1/4, 1/4 |

The symmetry-allowed values of the orbital angular momentum for fcc Al are 0, 4, 6, 8, 10, and 12. The smallest value, $l_{max} = 0$, uses the spherically symmetric component of the charge density only, and this choice can be considered as the best way to turn off the full-potential aspects of a full-potential method. The positions and values of the ELF bonding attractors as a function of $l_{max}$ are listed in Table 3. Total energies are also provided. The values $l_{max} = 0-6$ gave the same attractor positions; likewise, the results for $l_{max} = 8$ and 10 agree with the result of the full calculation with $l_{max} = 12$. Although the $l_{max} = 6$ calculation finds the same attractor locations as do the $l_{max} = 0$ and 4 ones, actually a different interconnectivity pattern is obtained for it. Thus, in Figure 3, we show the ELF isosurfaces computed with $l_{max} = 0$, 6, and 12 in the 1/8 of the cubic cell.

The result of the spherically symmetric ($l_{max} = 0$) FPLO calculation gives ELF valence attractors at (48*g*) *x*, 1/4, 1/4 positions, where $x = 0.055$. Because the (24*d*) 0, 1/4, 1/4 positions correspond to the midpoints of the closest Al−Al contacts, the $l_{max} = 0$ results can be regarded as (24*d*) positions being split. This view is consistent with the fact that the ELF value at the (24*d*) basin interconnection points (i.e., saddle

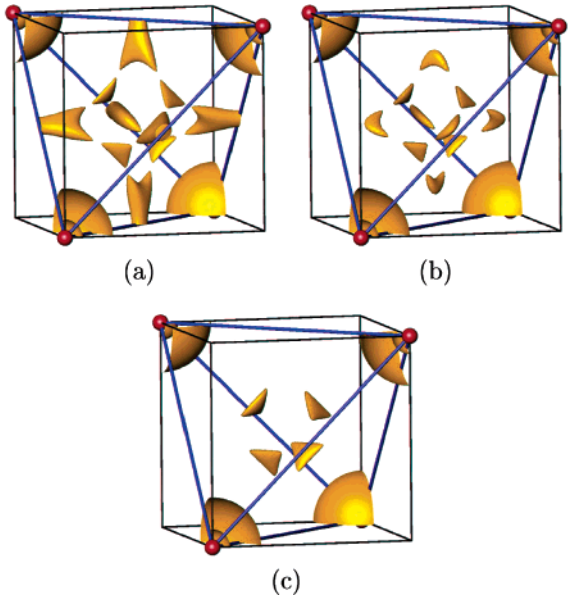


**Figure 3.** ELF isosurfaces in Al computed with (a) $l_{max} = 0$ ($\eta = 0.613$), (b) $l_{max} = 6$ ($\eta = 0.5975$), and (c) $l_{max} = 12$ ($\eta = 0.598$). Al atoms are shown by red spheres.

points) is very close to the attractor value, cf. Table 3. These (48*g*) attractors have disynaptic basins. There is a second set of attractors at (32*f*) *x*, *x*, *x* positions with $x = 0.19$. This value of *x* for the (32*f*) position is the same in all calculations reported in Table 3. The quantity $\Delta\eta^{a-bip}$, defined as the difference between the highest valence attractor value, $\eta^a$, and the lowest value of ELF occurring at valence basin interconnection points, $\eta^{bip}$, is very small having a value of $0.6170-0.6129 = 0.0041$. When $l_{max}$ is increased to 4, the order and the locations of the attractors and saddle points do not change but the difference in $\Delta\eta^{a-bip}$ increases to 0.0120. The $l_{max} = 6$ case forms an intermediate pattern: The attractors at (48*g*) [$x^{(48g)} = 0.095$] and (32*f*) positions have very close ELF values; therefore, one obtains a reducible domain first inside the octants, and the localization domains of neighboring octants join at (24*d*) positions at a smaller ELF value ($\eta = 0.5915$). Starting with $l_{max} = 8$, the ELF topology converges; the locations of the attractors and saddle points together with the order of their ELF values are the same for $l_{max} \geq 8$. Note also that the total energy at $l_{max} = 8$ is within 1 $\mu E_h$ of the converged value of the total energy.

Next, we considered the effects due to changes in the basis sets and the confining potential. Regarding the former, additions to the standard basis set were used as follows: (a) 4*f*, (b) 4*d*, (c) 4*s* 4*p*, and (d) 4*s* 4*p* 4*f*. For the latter, different values between 3.0 and 6.0 were chosen for the exponent *N*. We ended up with a large set of calculations by combining different *N* values with different basis sets. However, a converged result for the ELF topology did not emerge from these quite extensive calculations. Rather, the results kept changing between two cases: (i) single set of attractors located at (32*f*) and (ii) two sets of attractors located at (48*g*) and (32*f*) positions. Actually, in both cases, both positions (32*f*) and (48*g*) show up as locations of ELF critical points. However, although (32*f*) positions always appear as local maxima, (48*g*) positions are obtained as either local maxima or saddle points, and this forms the basic difference between the two cases.

Therefore, we studied the regions around the (48*g*) positions more closely. It turns out that the ELF distributions in these parts of the unit cell are very flat in the FPLO calculations. In particular, the value of the local ELF maximum at a (48*g*) site is only about 0.01 higher than the ELF values at nearby saddle points. As a result, conversion of such a small peak (along one of the principal axes) into a small well requires very small changes in the ELF values. So, although the ELF values themselves are converged to better than 0.01, the nature of the critical point at (48*g*) keeps changing between a local maximum and a saddle point because of this flatness of the ELF distribution. In the TB-LMTO-ASA calculation, on the other hand, the local maximum at the nearest-neighbor midpoint is a well-defined peak and the ELF distribution is not flat in the surrounding regions.

We, then, examined the situation from the viewpoint of energetics. The total energies of the calculations that produced these results differ from one another by less than 0.5 $\mu E_h$. Therefore, we have many energetically equally well-converged FPLO calculations, which predict either of the two results indicated above. Because the energy differences are quite small, it is not possible to prefer the result of one particular calculation over that of others by using total energy as a criterion.

In all of these calculations, the basins of the (32*f*) attractors are monosynaptic while those of the (48*g*) ones are disynaptic. Each monosynaptic basin holds about 0.36 electrons in the cases where only a single set of attractors are obtained. This implies about 2.92 valence electrons per Al atom. When there are two sets of attractors, the disynaptic basins contain most of the valence charge. In this category, we can identify two major types of results: (i) $\eta^a_{(48g)} > \eta^{bip}_{(24d)} > \eta^a_{(32f)}$ (similar to the $l_{max} = 0$ and 4 cases; Table 3 and Figure 3a) and (ii) $\eta^a_{(48g)} \sim \eta^a_{(32f)} > \eta^{bip}_{(24d)}$ (similar to the $l_{max} = 6$ case; Table 3 and Figure 3b). In the former case, the monosynaptic basins are very small and they typically hold about 0.012 electrons per basin; the disynaptic basins each have about 0.235 electrons. These numbers add up to approximately 2.92 valence electrons per Al atom. In the latter case, the basin populations become ~0.07 and 0.195 electrons per monosynaptic and disynaptic basins, respectively. The total number of valence electrons is similar to the above values.

Recently, we learned of another full-potential implementation of ELF.[31] Our preliminary calculations with version 0.9.26 of this FP-LAPW code[31] on Al found two sets of attractors located at (48*g*) and (32*f*) positions. The (48*g*) locations, *x*, 1/4, 1/4, have a very small *x* value; therefore, the amount of splitting from the nearest-neighbor midpoints, (24*d*) 0, 1/4, 1/4 positions, is smaller than what FPLO calculations obtain. The ELF attractors at the (32*f*) locations seem to be a *full-potential* feature; they appear in both of the full-potential implementations whereas the TB-LMTO-ASA method does not obtain them.

At this point, the significance of the (32*f*) attractors is not clear. A possible explanation can be suggested by assuming the existence of multicenter bonds in Al. In an fcc elemental metal, two probable locations for attractors with polysynaptic basins are (i) (4*b*) 1/2, 1/2, 1/2 and (ii) (8*c*) 1/4, 1/4, 1/4. The former corresponds to the center of an octahedral hole and implies six-center bonds. The latter locations are the centers of tetrahedral holes implying four-center bonds. The (32*f*) *x*, *x*, *x* locations obtained by full-potential calculations for Al can be interpreted as an indication that if multicenter bonds exist in Al, then the corresponding ELF attractors will most probably be located at the (8*c*) positions. Because the *x*, *x*, *x* positions can be regarded as 1/4, 1/4, 1/4 positions each split into four, one can view the full-potential results as an improvement over the ASA calculation toward a picture of multicenter bonding. However, as of now, there are no rules or theorems that enable us to predict the locations of ELF bonding attractors in advance. Hence,

whether the (32*f*) locations are indeed a part of the correct answer or they are a step toward it cannot be decided with currently available tools. Resolution of this matter certainly deserves more theoretical and computational work.

## 4. Summary

We have implemented ELF in the full-potential electronic structure code FPLO. This implementation has various advantages: (i) no shape approximations to the potential, (ii) uniform treatment of charge density and potential in all space (no muffin tin spheres), and (iii) numerically efficient because of the minimal basis approach. This last feature makes accurate calculation of ELF possible for systems with up to about 100 atoms in the unit cell. For larger systems (more than 100 atoms in the unit cell), TB-LMTO-ASA is still the method of choice due to memory and time constraints.

There are minor differences between the FPLO and the TB-LMTO-ASA results in structures with directed bonding (two-center bonds). On the other hand, in the structures of elemental metals, different ELF topologies are found in the valence region. Further studies on both simple and complex structures are necessary in order to obtain a better idea about the effects of full-potential treatment on ELF.

**Acknowledgment.** We are grateful to Professor C. Ambrosch-Draxl and Dr. J. K. Dewhurst for making available to us a developer release version of their EXCITING code. A.O. and H.R. thank the DFG (Emmy Noether program) for financial support.

## References and Notes

(1) Becke, A. D.; Edgecombe, K. E. *J. Chem. Phys.* **1990**, *92*, 5397.
(2) Savin, A.; Jepsen, O.; Flad, J.; Andersen, O. K.; Preuss, H.; v. Schnering, H. G. *Angew. Chem., Int. Ed. Engl.* **1992**, *31*, 187.
(3) Savin, A.; Nesper, R.; Wengert, S.; Fässler, T. F.; *Angew. Chem., Int. Ed. Engl.* **1997**, *36*, 1808.
(4) Gatti, C. *Z. Kristallogr.* **2005**, *220*, 399.
(5) ELF website: http://www.cpfs.mpg.de/ELF.
(6) Kohout, M. *Int. J. Quantum Chem.* **2004**, *97*, 651.
(7) Silvi, B.; Savin, A. *Nature* **1994**, *371*, 683.
(8) Hohenberg, P.; Kohn, W. *Phys. Rev.* **1964**, *136*, B864.
(9) Koepernik, K.; Eschrig, H. *Phys. Rev. B* **1999**, *59*, 1743.
(10) (a) Andersen, O. K. *Phys. Rev. B* **1975**, *12*, 3060. (b) Andersen, O. K.; Jepsen, O. *Phys. Rev. Lett.* **1984**, *53*, 2571.
(11) Jepsen, O.; Andersen, O. K. *The Stuttgart TB-LMTO-ASA Program*, version 4.7; Max-Planck-Institut für Festkörperforschung: Stuttgart, Germany: 2000. The ELF module is already included in this version.
(12) Eschrig, H. *Optimized LCAO Method and the Electronic Structure of Extended Systems*; Springer: Berlin, 1989.
(13) Blaha, P.; Schwarz, K.; Madsen, G. K. H.; Kvasnicka, D.; Luitz, J. *WIEN2k, An Augmented Plane Wave Plus Local Orbitals Program for Calculating Crystal Properties*; Vienna University of Technology: Austria, 2001.
(14) Rosner, H.; Divis, M.; Koepernik, K.; Drechsler, S.-L.; Eschrig, H. *J. Phys.: Condens. Matter* **2000**, *12*, 5809.
(15) Rosner, H.; An, J. M.; Pickett, W. E.; Drechsler, S.-L. *Phys. Rev. B* **2002**, *66*, 024521.
(16) For a list of publications and more detailed information, see http://www.fplo.de.
(17) Kohn, W.; Sham, L. J. *Phys. Rev.* **1965**, *140*, A1133.
(18) Perdew, J. P.; Wang, Y. *Phys. Rev. B* **1992**, *45*, 13244.
(19) von Barth, U.; Hedin, L. *J. Phys. C* **1972**, *5*, 1629.
(20) Perdew, J. P.; Zunger, A. *Phys. Rev. B* **1981**, *23*, 5048.
(21) Jepsen, O.; Andersen, O. K. *Z. Phys. B.* **1995**, *97*, 35.
(22) Kohout, M. *Program Basin*, version 2.4; Max-Planck Institut für Chemische Physik fester Stoffe: Dresden, Germany, 2004.
(23) Kittel, C. *Introduction to Solid State Physics*, 7th ed.; John Wiley and Sons: New York, 1996; p 23.
(24) Donahue, J. *The Structures of the Elements*; John Wiley and Sons: New York, 1974; pp 254−256.
(25) Schmidt, J.; Schnelle, W.; Grin, Y.; Kniep, R. *Solid State Sci.* **2003**, *5*, 535.
(26) Pauling, L. *The Nature of the Chemical Bond*, 3rd ed.; Cornell University Press: Ithaca, 1960.
(27) Silvi, B.; Gatti, C. *J. Phys. Chem. A* **2000**, *104*, 947.
(28) It should be noted that the purpose of current study is *not* to analyze the nature of the metallic bond. Here, we are mainly concerned with possible changes in ELF topology in a few selected crystalline materials due to full-potential treatment. However, we have tried to take the general chemical-bonding considerations into account as much as possible in selecting the examples.
(29) Pisani, C.; Dovesi, R.; Roetti, C. *Hartree−Fock Ab Initio Treatment of Crystalline Systems*; Lecture Notes in Chemistry 48; Springer-Verlag: Berlin, 1988.
(30) Silvi, B. *J. Mol. Struct.* **2002**, *614*, 3.
(31) Dewhurst, J. K.; Sharma, S.; Ambrosch-Draxl, C.; Brouder, Ch. *Full-Potential Linearised Augmented-Planewave Code EXCITING for Determining the Properties of Crystalline Solids*, version 0.9.26; University of Graz: 2005.